Development of MRI-based Yucatan Minipig Brain Template

Caroline Nicole Norris

Thesis submitted to the faculty of the Virginia Polytechnic Institute and State University in partial fulfillment of the requirements for the degree of

Master of Science
in
Biomedical Engineering

Pamela J. VandeVord, Chair
Stephen M. LaConte, Co-Chair
Michael J. Friedlander
Elizabeth M. McNeil

March 27, 2019
Blacksburg, Virginia

Keywords: Yucatan, MRI, brain, template

Development of MRI-based Yucatan Minipig Brain Template

Caroline Nicole Norris

ABSTRACT

Yucatan minipigs have become increasingly common animal models in neuroscience where recent studies, investigating blast-induced traumatic brain injury, stroke, and glioblastoma, aim to uncover brain injury mechanisms [1-3]. Magnetic Resonance Imaging (MRI) has the potential to validate and optimize unknown parameters in controlled populations. The key to group-level MRI analysis within a species is to align (or register) subject scans to the same volumetric space using a brain template. However, large animal brain templates are lacking, which limits the use of MRI as an effective research tool to study group effects. The objective of this study was to create an MRI-based Yucatan minipig brain template allowing for uniform group-level analysis of this animal model in a standard volumetric space to characterize brain mechanisms. To do this, 5-7 month old, male Yucatan minipigs were scanned using a 3 Tesla whole-body scanner (Siemens AG, Erlangen) in accordance with IACUC. T1-weighted anatomical volumes (resolution = $1\times1\times1$ mm^3; TR = 2300 ms; TE= 2.89 ms; TI = 900 ms; FOV = 256 mm^2 ; FA = 8°) were collected with a three-dimensional magnetization prepared rapid acquisition gradient echo (MPRAGE) pulse sequence [4]. The volumes were preprocessed, co-registered, and averaged using both linear and non-linear registration algorithms in AFNI [5] to create four templates (n=58): linear brain, non-linear brain, linear head, and non-linear head. To validate the templates, tissue probability maps (TPMs) and variance maps were created, and landmark variation was measured. TPMs computed in FSL [6] and AFNI show enhanced tissue probability and contrast in the non-linear template. Additionally, variance maps showed a more uniform spatial variance in the non-linear template compared to the linear. Registration variation within the brain template was within 1.5 mm and displayed improved landmark variation in the non-linear brain template. External evaluation subjects (n=12), not included in the template, were registered to the four templates to assess functionality. The results indicate that the developed templates provide acceptable registration accuracy to enable population comparisons. With these templates, researchers will be able to use MRI as a tool to further neurological discovery and collaborate in a uniform space.

Development of MRI-based Yucatan Minipig Brain Template

Caroline Nicole Norris

GENERAL AUDIENCE ABSTRACT

Magnetic resonance imaging (MRI) is commonly used in neuroscience as a non-invasive diagnostic tool with the potential to reveal unknown brain injury mechanisms. MRI is particularly useful in large animal models to validate and optimize unknown parameters in controlled populations. The key to group-level MRI analysis within a species is to align (or register) subject scans to the same volumetric space using a brain template. However, large animal brain templates are lacking, which limits the use of MRI as an effective research tool to study group effects. The objective of this study was to create an MRI-based Yucatan minipig brain template allowing for uniform group-level analysis of this animal model in a standard volumetric space to better characterize brain mechanisms. The neuroanatomy of the Yucatan minipig, which is characterized by an increased brain size and gyrencephalic intricacies similar to humans, has made it an increasingly common animal model in neuroscience. Linear and non-linear registration methods were performed in Analysis of Functional NeuroImages (AFNI) software to create both brain and head templates for 5-7 month old, male Yucatan minipigs (n=58). This study was validated looking at template variance, tissue probability maps (TPMs) of segmented grey matter, white matter, and cerebrospinal fluid, and landmark variation. The results indicate that the developed templates provide acceptable registration accuracy to enable population comparisons. With these templates, researchers will be able to use MRI as a tool to further neurological discovery and collaborate in a uniform space.

Acknowledgements

I would like to acknowledge the Department of Biomedical Engineering and Mechanics and the Center for Injury Biomechanics at Virginia Tech for supporting this research. This work was partially funded by the Office of Naval Research Contract N00014-14-C-0254.

Thank you to my family and friends for your daily words of wisdom and encouragement. I would not be where I am today without your love and support. I would like to thank the entire Department of Biomedical Engineering and Mechanics for the collective faculty support over these past years. I truly appreciate your time and devotion to teaching, which feeds my love of learning. I would like to thank Dr. Brad Hubbard and Shaylen Greenberg for being incredible mentors, always improving my mood, and for leading by example. I will always look up to you. Additionally, thank you to the members of the VandeVord and LaConte labs for your professional and emotional guidance on any given day. I cannot thank you enough, Jonathan Lisinski, for your kindness, quick replies, and constant enthusiasm for problem solving in AFNI.

Furthermore, I am thankful for my committee members, without whom this project would not be possible. Thank you, Dr. Michael Friedlander, for your neuroscience expertise and your time throughout this process. To Dr. Elizabeth McNeil, thank you for introducing me to this project and expanding my intellectual curiosity in ways I never thought possible. To Dr. Stephen LaConte, thank you for taking the time to help me grow as a researcher and for sharing your passion for neuroimaging. And lastly, but most importantly, to Dr. Pamela VandeVord, thank you for your guidance and dedication to this project and thesis. You took a chance on me, recognizing my potential, and for that, I can't thank you enough.

Table of Contents

List of Figures

List of Tables

List of Abbreviations

Abbreviation	Meaning
General	
MPRAGE	Magnetization Prepared Rapid Acquisition Gradient Echo
MRI	Magnetic Resonance Imaging
SNR	Signal to Noise Ratio
TPMs	Tissue Probability Maps
Software	
AFNI	Analysis of Functional NeuroImages
FSL	Functional magnetic resonance imaging of the brain's (FMRIB's) Software Library
SPM	Statistical Parametric Mapping
Templates	
T_{LB}	Linear Brain Template
T_{NLB}	Non-Linear Brain Template
T_{LH}	Linear Head Template
T_{NLH}	Non-Linear Head Template
Landmarks	
AC	Anterior Commissure
HN	Habenular Nuclei
PC	Posterior Commissure

Introduction

Brain templates play a critical role in data analysis and interpretation of neuroimages across populations of interest. Digital brain templates are used in conjunction with neuroimaging modalities, such as magnetic resonance imaging (MRI), with the purpose of aligning (or registering) subject scans within a population of interest to the same volumetric coordinate space. After registering to template space, group-level statistical analysis may be performed to interpret population data. MRI-based templates are closely associated with human brain atlases, or volumetric maps of internal brain regions. Often the terms "atlas" and "template" are used interchangeably [7], however for the purposes of this study we will note that the template refers to coordinate recognition and standardization of orientation while the atlas contains the specific spatial data of the subject within the template frame. The atlas works in series with the template and together they enhance the information that can be extracted from neuroimages, ultimately allowing for uniform processing.

Uniform processing of neuroimages across a patient population is important because it provides a frame of reference. However, the data extracted from neuroimaging modalities for a population of interest is not uniform due to misalignment and movement in the scanners, anatomical differences between patients, and underlying processing artifacts from the scanners. To correct these offsets, data from each scan is aligned (or registered) to a brain template, placing them in the same volumetric space. Within a standard space, voxel-wise, region-of-interest, and network analyses can be performed to understand functional properties [7]. This information paired with spatial referencing, provided by the brain atlas, standardizes the analysis process across patients as well as research groups.

Human templates and atlases are created based on stages of development and brain structure. The maturational progress of the human population of interest must be considered as many variables necessary for neuroimage analysis are constantly changing [7-11]. For example, just after birth, signal intensity profiles shown in brain MRI are altered due to reduced water content and increased cell density. The perinatal brain will also exhibit reduced spatial resolution and tissue contrast compared to adults [7, 12]. On the other hand, as populations mature, MRI-based studies have found that the brain experiences atrophy of grey and white matter along with the expansion of lateral ventricles and sulci spaces at varying rates [7, 13-15]. In addition to age, other factors such as sex, ethnicity, medical history, and cognition must be taken into account when assessing stages of brain development [7, 16, 17]. In a study by Fillmore et al. (2015), age-specific templates were created for healthy adults between 20 to 89 years. It was found that individual subject data showed closer alignment to the age-specific templates than to the templates of greater age

ranges [18]. As expected, registration is more precise among controlled populations with similar signal intensity profiles, spatial resolution, tissue contrast, and tissue volume.

For years, studies have developed and refined human templates and atlases as a tool for research understanding and medical diagnosis. However, human brain injury studies using MRI lack the experimental controls necessary to validate findings. Animal models provide a way to fill this research gap. Swine models, for example, are commonly selected in neuroscience research due to similarities of pig brains to human brains [19]. Since the 1960s, pig brain growth has been studied with notable similarities in the neonatal porcine brain compared to the human infant brain. Extensive publications detailing the species-specific physiology of pigs and their similarities to humans have verified the usefulness of swine models in neuroscience applications over rodents. Even more, pigs are preferred to nonhuman primates due to their life span of 12-15 years, simple breeding and larger litter sizes, shorter gestation periods of around 113-115 days, and quick maturation within the first 3-6 months depending on the breed. Agricultural pigs are ideal for acute research studies at low weights (around 40 kg), which in turn limits the age usage to less than 6 weeks old [20]. A rapidly increasing laboratory model in the field of neuroscience was developed using minipigs, known to have substantial genetic likeness to humans [21, 22].

Miniature breeds, most commonly Hanford, Yucatan, Sinclair, and Göttingen (from largest to smallest), vary in size and development of organs, yet the physiologic function of the organs can be age-matched for comparison between breeds [19, 23]. Because Göttingen minipigs are the smallest, reaching an adult size of 35-55 kg, data for this breed is more readily available over others [20, 24]. However, for neuroimaging applications, increased subject size is preferred making Yucatan minipigs (adults reaching 70-90 kg) a more suitable animal model [20]. Brain imaging of this particular breed using computer tomography (CT), brain positron emission tomography (PET), and MRI is not a novel approach as stereotaxic localization methods have been in use for about a decade [25]. A particular study by Khoshnevis et al. (2017) looked at implanted human glioblastoma growth in Yucatan minipigs using CT scans and indicated that the Yucatan model has a high compatibility with the imaging platform similar to that of the human stereotaxic frame [2]. In addition, a paper by Platt et al. (2014) used MRI to quantify regions of brain ischemia following a stroke using histology to support the MRI data [3]. The supporting histological data was necessary because even though imaging modalities are widely used on this breed, a standard brain template for automatic registration is not available. To further explore the potential of this animal model as a means to uncover the unknowns of neuroscience, the objective of this study is to develop an MRI-based brain template for the Yucatan minipig.

Literature Review

Template Space

Since the early 1900's scientists have worked to document and map the landscape of the human brain. As technologies improved, Jean Talairach developed a three-dimensional coordinate space in 1967, which was later updated in 1988 with the help of Pierre Tournoux to create the Talairach-Tournoux coordinate space (most commonly referred as Talairach space). Talairach space is dependent on the manual identification of the anterior commissure (AC) and the posterior commissure (PC) landmarks where the horizontal axis is defined as the line intersecting the AC and PC (known as the AC-PC line). Directly following the Talairach space definition, Fox et al. (1985) was able to apply transformations (translational and rotational) to collected PET image data to map individuals to the same space. This novel idea led to the publication of structural MRI templates with the ability to analyze data across subjects in the same space [26].

Evans et al. (1992), was one of the first studies to implement the fundamental steps of template creation: AC-PC alignment to Talairach space, co-registration to a volume of interest, and averaging of voxels from different subjects into a merged dataset. In this study, 37 T1-weighted MRI volumetric datasets were fitted to the AC-PC line using an image software tool. Next, each subject was co-registered to a volume of interest by applying a piecewise linear transformation to selected brain landmarks in Talairach space. All subjects, now in the same volumetric space and orientation, were averaged in a voxel-wise manner to merge all 37 datasets into one template space. Blurriness of the resulting template was an indicator of how well the initial transformations were applied, which needed to be optimized or else template functionality decreased [27].

Many techniques have been performed to optimize template creation since the 1990's. It was found that after the AC-PC alignment, co-registration to a single volume, and averaging of the co-registered volumes in Talairach space, a second iteration of the co-registration and averaging steps is necessary to reduce effects from manual errors and provide a sharper average. In the second iteration, all MRI image volumes are co-registered to the template created in the first iteration. This can either remain in Talairach space using registration with Talairach's piecewise linear model to selected landmarks, or a separate transformation matrix can be applied using either linear or non-linear algorithms for optimized co-registration [26]. When linear or non-linear algorithms are applied in the co-registration step, the coordinates are no longer in Talairach space, but are instead transformed to a space defined by the Montreal

Neurological Institute (MNI space). This coordinate space has been used as the basis for human brain template space ever since.

Template Quality

In a study by Collins et al. (1994), automatic registration techniques in MNI space were found to be more efficient with reduced standard deviation compared to piecewise linear registration to manually selected landmarks. Major drawbacks of manual landmark selection for registration to Talairach space include increased time, decreased reproducibility, increased interobserver variability, and difficulty of intrasubject landmark matching due to varied imaging parameters and patient position within the scanners. This study served to create algorithms that optimized voxel-to-voxel comparisons regardless of the original imaging parameters or orientation. The first well-known human template in MNI space was composed of 305 human brains averaged into one volumetric space using a linear 9-parameter whole-brain mapping algorithm (MNI305). The 9-parameters included coefficients of translation, rigid body rotation, and anisotropic scaling in three dimensions. These parameters were generated using automatic edge detection based on changes in intensity and gradient magnitude which corresponded to internal anatomical structures. Collins et al. (1994) also found that registration was improved by manually creating a brain mask to remove the scalp, skull, or meninges from the MRI volumes (also known as skull-stripping). It was found that these external factors introduced bias in subject transformations due to signal intensity inhomogeneities surrounding the brain. Another key to improving registration capabilities was to apply intensity correction after creating the brain mask to help boundaries between tissue types stand out during edge detection [28].

Since the development of the MNI305, other well-known templates such as the MNI152 and ICBM 452 have been created in attempts to improve resolution, contrast, and signal-to-noise ratio. The MNI152 decreased the sample size of the subjects (n=152) and narrowed age ranges to obtain an improved template with higher resolution and better structural contrast. The ICBM 452, on the other hand, increased the number of subjects to 452 and applied both a linear 12-parameter transformation and a 5th-order polynomial non-linear warping function [26]. The 12-parameter transformation involves translation, rotation, and scaling along both orthogonal and nonorthogonal axes. Non-linear warping functions were developed to maintain high-dimensional anatomical accuracy due to specialization of the function in localized regions [29]. Despite its required increase in processing time and power, non-linear methods increase degrees of freedom, resulting in an increased robustness of the registrations. This is mainly due to the non-linear, non-isometric variability of anatomical structures from one subject to the next [26, 28]. These non-linear methods used in conjunction with increased sample size also increases signal-to-noise ratio. Likewise,

increasing the number of registration iterations in conjunction with the application of non-linear algorithms has been shown to increase spatial resolution [26].

Some might ask, why increase the sample size if the resolution will be compromised? The importance of template sample size is to make sure that the intended population for template use is well represented. That is, if the template is intended for use on all genders, ages, and ethnicities, the population of internal template subjects should encompass an effective number from each category, increasing the total sample size. Conversely, if a study is to be conducted within a defined population constraint, it is best to use a template that is also well-defined based on the specific population of interest. For example, the study by Fillmore et al. (2015) mentions that study-specific templates are often generated by averaging all subject data into a template prior to analysis, rather than relying on larger population-based template options [18]. The general rule of thumb is to increase the number of subjects in the template if the signal-to-noise ratio is low. There will come a point where the signal-to-noise ratio will level out and the optimal subject population for the template will be determined [30]. All of these factors need to be taken into account when deciding which brain template will best represent the population of interest within a study and can have a major impact on determining significance of data between subjects.

Non-Human Templates

Previous studies have created non-human templates which follow the same general process: AC-PC align, skull-strip, normalize intensities, register to same space, and average the scans [31-36]. However, each step of the process is performed differently and in a different order depending on the types of scans available and the software packages used. Non-human templates started to develop around the same time as the human templates, but due to the vast number of animals, their unique anatomy, and popular demand, human templates have made much greater strides in template optimization. Specifically, imaging software now has optimized algorithms for skull-stripping, which, as previously mentioned, decreases registration bias and improves template quality [28]. For non-humans, manual skull-stripping is generally performed due to the inability of automated methods such as the Brain Extraction Tool (BET) in FSL or 3dSkullStrip in AFNI to distinguish between human and non-human brain structures. This manual brain selection introduces error and reduces efficiency of the overall template, which is a major drawback in non-human template creation. Another major drawback to non-human templates is that head templates are not typically available. A head template is a template with a high-resolution brain that also contains surrounding structures such as the skull and meninges. These templates are commonly used in humans and can be used

for registration without prior skull-stripping. Taking away the need for skull-stripping of non-human subjects is efficient and has the potential to reduce compounding error during analysis.

Two of the most common software packages used to create population-based templates in non-humans are FSL and SPM. [31-33, 35, 36]. In general, templates use SPM for registration and averaging, but make use of FSL for its ability to segment the brain into grey matter, white matter, and cerebrospinal fluid, using the FSL FAST segmentation function. These segmented tissue types can be averaged together across the subjects to create tissue probability maps (TPMs), which provide a closer look at the enhanced resolution of one template versus another by seeing how well the tissue types are represented on a probability scale from 0 to 1 [37]. TPMs are a method of validation that can also be used as templates for region of interest studies [34]. Another common validation method is a landmark measure. This is performed by selecting points of interest within a subject's brain, such as the AC or PC, and measuring the Euclidian distance (**Eq. 1**) between the subject and template landmarks [31, 32, 35]. Quality of the template is optimal when tissue probability maps have a high resolution and measured distances between landmarks are minimized.

$$d = \sqrt{(x - x_{true})^2 + (y - y_{true})^2 + (z - z_{true})^2} \quad (1)$$

While a volumetric MR atlas was created for the Yucatan minipig based on histology, the results did not provide any quantitative validation of the atlas, the atlas did not contain properties that can be used for spatial normalization, and the atlas was created with a low field strength of 1.5 Tesla and small sample size of n=6 [19]. Other MR templates with higher field strength and sample size exist for the domestic pig (*Sus scrofa*) [31, 38] and the Gottingen minipig [39], however the unique anatomical complexity across breeds limits registration quality of the Yucatan brain to these templates. The main aim of this study is to create Yucatan minipig brain and head templates which allow for accurate group-level analysis in a standard volumetric space for evaluation of unknown brain pathology using this animal model.

Methods

Image Acquisition

MR imaging of 5-7 month old, male Yucatan minipigs (n=72) was performed using a 3 Tesla whole-body scanner (Siemens AG, Erlangen) in accordance with the Institutional Animal Care and Use Committee (IACUC). Subjects were placed in the scanner in the supine position. The anesthesia and end-tidal CO_2 tubing was run through a waveguide in the control room along with a fiber-optic cable for the MRI-compatible pulse oximeter, passing approximately 4.6 cm from the wall to the scanner's isocenter. T1-weighted anatomical volumes (resolution = 1×1×1 mm^3; TR = 2300 ms; TE= 2.89 ms; TI = 900 ms; FOV = 256 mm^2 ; FA = 8°; BW = 140 Hz/pixel) were collected with a three-dimensional magnetization prepared rapid acquisition gradient echo (MPRAGE) pulse sequence [4].

Image Preprocessing

Files from the 72 subjects were converted from digital imaging and communications in medicine (DICOM) format to 3D volumes in HEAD/BRIK format for use in the Analysis of Functional Neuro-Images (AFNI) software [5]. All volumes were rotated to the AC-PC line using a semi-automated algorithm in AFNI that aligns the subjects based on five marker locations. The five markers were manually placed on the top middle of the anterior commissure, rear middle of the anterior commissure, bottom middle of the posterior commissure, and two points along the mid-sagittal plane for each subject. After a series of quality checks in the alignment interface, the scans were aligned in accordance with the Talairach space definition. Manual skull-stripping was then performed in AFNI by drawing a brain mask over individual image slices for all subjects. The underlying image volumes were then extracted from beneath the mask using the 3dcalc function. Prior to template generation, the intensity of the template subjects was normalized by the 3dUnifize function in AFNI to improve contrast scaling of the white and grey matter across the T1-weighted images. Refer to **Fig. 1** to review these preprocessing steps. At this stage, two subjects were excluded from the study due to low signal-to-noise ratio and visible artifacts within the T1-weighted scans. The remaining 70 subject scans were split into two groups such that 58 were used in template creation and 12 were used in template validation.

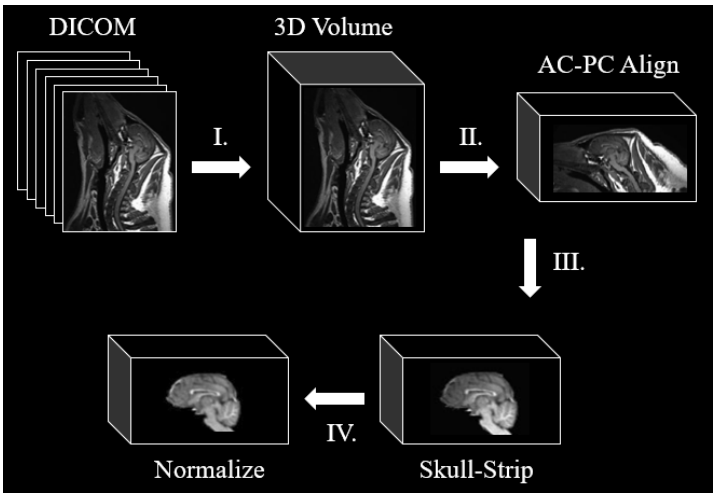

Figure 1. Preprocessing steps: **I)** Convert from DICOM to a 3D volume. **II)** Apply the AC-PC alignment algorithm. **III)** Manually skull-strip each volume. **IV)** Normalize image intensities.

Template Generation

A recursive method was implemented to create brain and head templates (n=58) using both linear and non-linear methods. A schematic of the brain and head template methods, described below, can be shown in **Fig. 2** and **Fig. 3**. The subject of average age and weight (5m, 17d and 20.6 kg) was chosen as the initial template (T_0). The remaining 57 preprocessed scans were individually registered to T_0 space. This was done using the 3dAllineate function in AFNI, which allows for a 12-parameter affine transformation and generates a linear transformation matrix, specific to each subject (${M_0}^n$). Then, the 3dMean function performed a voxel-wise average of all 58 subjects to create the first template (T_1). Starting the second iteration, the original preprocessed scans were individually registered to the T_1 space, generating a new 12-parameter linear affine transformation matrix for each subject (${M_1}^n$).

Linear Brain Template (T_{LB})*:* Once aligned to the T_1 space, the scans were voxel-wise averaged using 3dMean. *Non-Linear Brain Template* (T_{NLB})*:* A non-linear warping function, 3dQwarp, was applied to all scans after the linear transformation to the T_1 space. This warping uses Hermite cubic basis functions, generating splines of increasing order, to fit patched regions in steadily decreasing increments across the registered brain. These higher order warping functions were saved for each subject (W^n). The warped subjects were then averaged using 3dMean.

Linear Head Template (T_{LH})*:* The 12-parameter linear affine transformation matrix, ${M_1}^n$, was applied to each subject's AC-PC aligned full head scan (prior to skull-stripping). The full head scans were then averaged together using 3dMean. *Non-Linear Head Template* (T_{NLH})*:* Each subject's 12-parameter

linear affine transformation matrix, $M_1{}^n$, and non-linear warping function, W^n, generated during the creation of T_{LB} and T_{NLB}, was applied to the AC-PC aligned full head scans. The volumes were then voxel-wise averaged together using 3dMean.

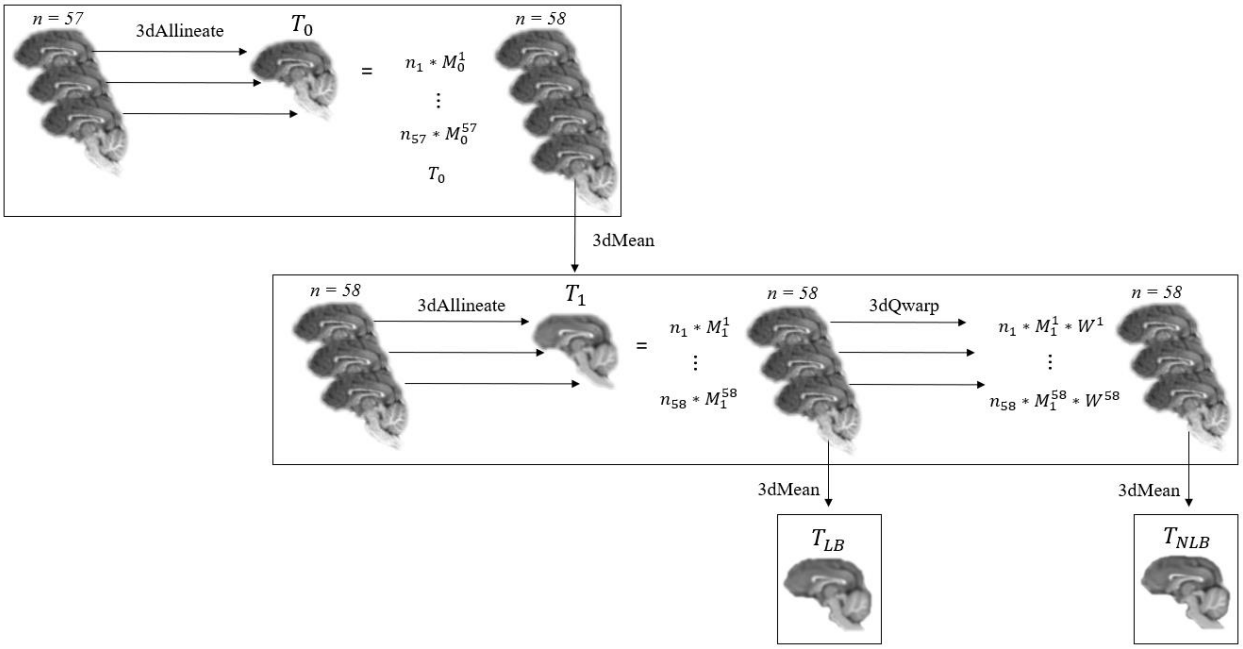

Figure 2. Brain template iterative method using linear and non-linear registration steps in AFNI.

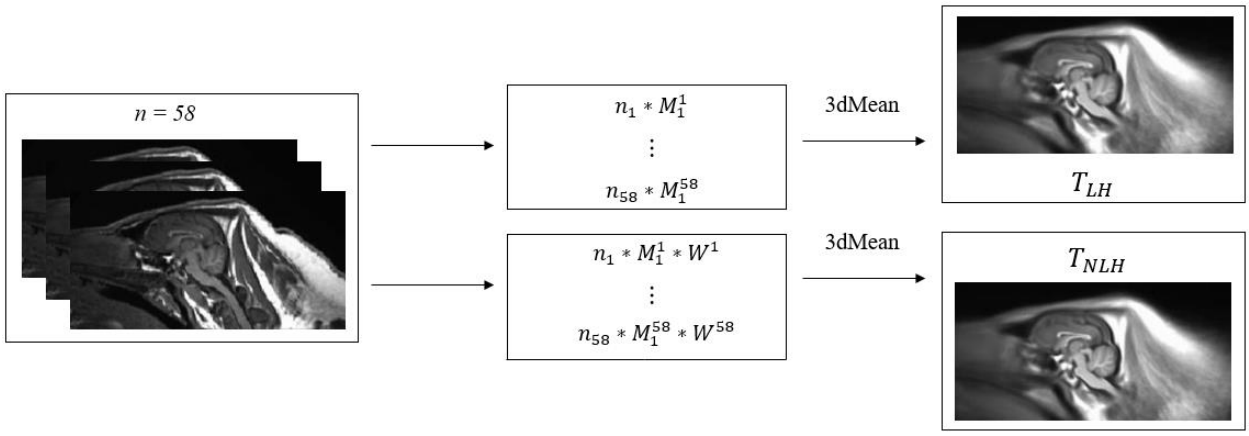

Figure 3. Head template method applying linear and non-linear transformations to AC-PC aligned full head scans.

Tissue Probability and Variance Maps

Tissue Probability Maps: The 58 skull-stripped, AC-PC aligned subject scans were converted to NeuroImaging Informatics Technology Initiative (NIFTI) format for use in FSL [6]. Tissue segmentation was performed for each subject using FMRIB's Automated Segmentation Tool (FSL FAST), segmenting into three tissue types: cerebrospinal fluid (CSF), grey matter (GM), and white matter (WM). The files were converted back to HEAD/BRIK format for use in AFNI and each subject's respective transformation matrix ${M_1}^n$ was applied to each tissue type. The voxel intensities were normalized from 0 to 1 within each file and the 58 files for each tissue type were averaged using 3dMean to create the linear CSF, GM, and WM tissue probability maps (TPMs) for validation of T_{LB}. Non-linear tissue probability maps were created from a similar process, however, instead of only applying the ${M_1}^n$ linear matrix, the W^n non-linear warping function was also applied prior to normalization and averaging.

Variance Maps: Brain template voxel-wise intensity variance was measured in the T_{LB} and T_{NLB}. This was performed using the *-stdev* option within the 3dMean function in AFNI to extract the voxel-to-voxel standard deviation between subjects averaged together in the template. The voxel-wise output was squared to provide a variance, which was then normalized from 0 to 1 for both brain templates in order to view the spatial variance across each template.

Landmark Validation

Three landmarks were selected as distinct locations in the brain: the anterior commissure (AC), posterior commissure (PC), and habenular nuclei (HN). Three points, directly at the centroid of the AC, PC, and HN, were manually selected in all 70 subjects. This was carried out using the drawing plugin in AFNI to create a single-voxel mask. Two methods of validation were performed: for internal template subjects and external evaluation subjects. Internal template subject landmark variation was performed to assess the variation of the 58 landmarks within the brain templates. In other words, it is a measure of the internal template error. The external landmark variation was performed to assess the functionality of the four created templates on the 12 evaluation subjects that were not included in the template. Analysis was performed in MATLAB version R2018b.

Internal Template Landmark Variation: The respective transformation matrices, ${M_1}^n$, were applied to the AC, PC, and HN points for each internal template subject to transform it to the linear template space (T_{LB}). These transformed points were used for linear validation. To validate the non-linear brain template, the warping functions, W^n, were applied to the single voxels directly following the ${M_1}^n$

transformation. This caused dispersion of a single voxel into multiple. The average voxel location was calculated for each landmark in non-linear brain template space (T_{NLB}). Averages of the x, y, and z coordinates were calculated across all 58 subjects to determine the true landmark location in the template space. The Euclidian distance (d) was measured (in mm) from each landmark point in T_{LB} and T_{NLB} space to the calculated true landmark location using **Eq. 1**.

External Subject Landmark Variation: The 12 skull-stripped volumes of the evaluation subjects were linearly registered to the brain templates (T_{LB} and T_{NLB}), using the 3dAllineate function. Similarly, the 12 full head scans of the evaluation subjects were registered to the head templates (T_{LH} and T_{NLH}). Four linear transformation matrices for each subject were generated from these registrations and applied to the AC, PC, and HN landmarks in original space to get to the respective template space. The Euclidian distances (d) were measured (in mm) from each subject's transformed landmark point to the true landmark location using **Eq. 1**.

Statistics

All statistical analysis was performed in MATLAB version R2018b. Significance of internal template landmark variation was determined using a Mann-Whitney U test such that the data does not follow a normal distribution around the mean landmark location. Normality was checked using the Shapiro-Wilk test. The average distance from each transformed landmark to the true landmark was compared for the linear brain template versus the non-linear brain template where $p < 0.05$ was significant. The *ranksum* function in MATLAB was used to test the significance between the two groups at each landmark.

The non-parametric Wilcoxon signed rank test for paired populations was performed to determine significance of external subject registration for the brain templates versus the head templates. The distances of the external subject landmarks to the true mean, following registration to the brain template, were compared to the distances of the head template landmarks around that same mean. The *signrank* function was used to test significance between the two groups at each landmark where $p < 0.05$ was significant.

Results

Linear brain (T_{LB}), non-linear brain (T_{NLB}), linear head (T_{LH}), and non-linear head (T_{NLH}) templates were created. As shown in **Fig. 4** below, the brain and its internal structures are distinct in all four templates. Further evidence can be seen in **Fig. A1** – **Fig. A4** in Appendix A. In the head templates, the regions inside the brain are much more distinct than the external structures, as expected. In addition, there is a noticeable improvement in resolution of the white matter tracts in the non-linear templates compared to the linear templates.

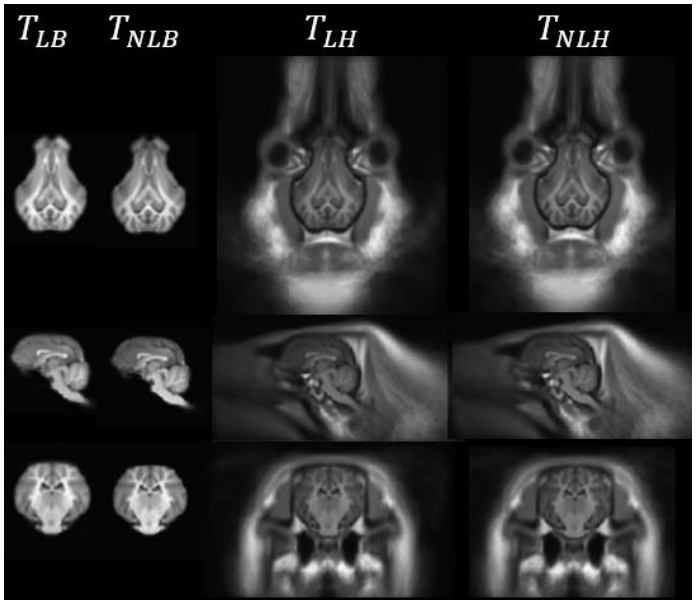

Figure 4. Axial, sagittal, and coronal views of the linear brain (T_{LB}), non-linear brain (T_{NLB}), linear head (T_{LH}), and non-linear head (T_{NLH}) templates.

Tissue Probability and Variance Maps

The created maps provide scales for visual comparison of segmented tissue probability and voxel intensity variance in the linear versus the non-linear templates. In the TPMs (**Fig. 5**), the main differences can be seen along the edges of the tissue types where the tissue probability increases in the non-linear template, thus increasing its contrast against the black background. With this increase in contrast, the intricacies of the internal brain structure are enhanced. Likewise, the main differences in the variance maps of the linear whole brain template versus the non-linear template can be found along the edges (**Fig. 6**). However, in this case, the linear brain template has a greater magnitude of voxel intensity variance, shows a greater percentage of variance along the outer edges, and has little to no variance in the internal brain

structure. The non-linear template shows improved spatial distribution of variance across the whole brain such that the variance of the internal structures is well represented by the subject population and the variance along the outer edges has been reduced.

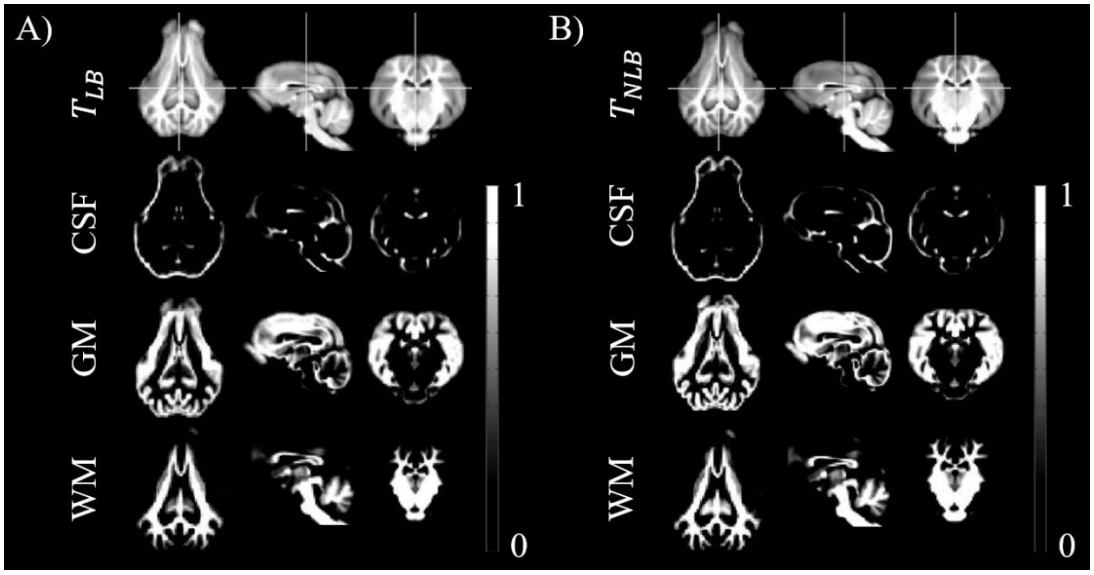

Figure 5. Tissue probability maps: **A)** Linear brain template (T_{LB}) and **B)** Non-linear brain template (T_{NLB}). Maps of cerebrospinal fluid (CSF), grey matter (GM), and white matter (WM) values range from 0 to 1 where 0 indicates that the tissue type was not present in any subjects at that voxel location and 1 indicates that the tissue type was represented in that location for all subjects included in the template population.

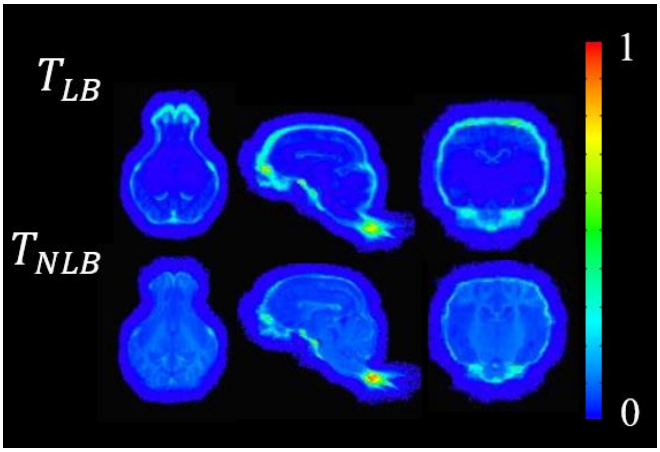

Figure 6. Variance maps of the linear brain template (T_{LB}) and non-linear brain template (T_{NLB}) where 0 represents regions of low voxel variance between subjects and 1 represents regions of high voxel variance between subjects.

Internal Template Landmark Variation

Single voxels located directly at the centroid of the AC, PC, and HN were manually selected in both the T_{LB} and T_{NLB} templates in AFNI, as shown in **Fig. 7**. Due to the 1×1×1 mm^3 resolution of the scans, the selected landmark coordinates are fit to the nearest whole millimeter. The error of this fit is provided in **Table 1** as the distance from the true floating-point coordinate location in the T_{LB} and T_{NLB} templates to the coordinates rounded to the nearest millimeter in AFNI. The true coordinate location was calculated as the average of the internal subject landmarks transformed to both linear template space and non-linear template space. This error ranges from 0.34 mm to 0.56 mm and should be considered when manually selecting brain features in template space.

After the transformation matrices and warping functions were applied to the selected landmarks in original space, the floating-point locations of the 58 subject landmarks in the linear and non-linear brain template spaces were plotted. The distribution of these transformed points around the true average coordinate location (blue dot) can be seen in **Fig. 8** to **Fig. 10**. The average and maximum distances from the subject landmarks to the true average coordinate location are reported in **Table 2**. Across all landmark locations, the difference between the linear and non-linear internal landmark variation was not found to be significant. However, the mean and maximum distances from the true location decreased in the non-linear brain template space compared to the linear brain template space, as did the variance around the mean.

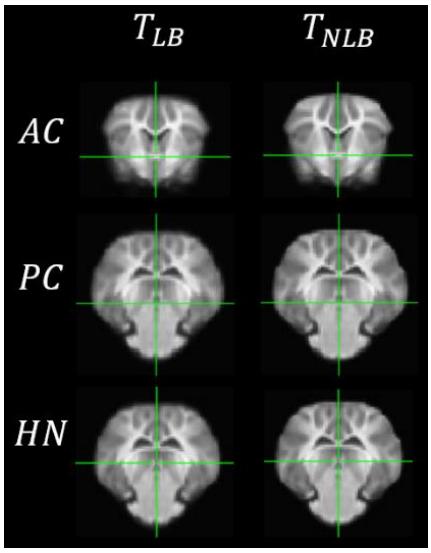

Figure 7. Selected landmarks for validation in the linear and non-linear brain templates: anterior commissure (AC), posterior commissure (PC), and habenular nuclei (HN).

Table 1. Internal subject landmark error from manual selection in brain template space.

		Template Coordinate			True Coordinate			Distance
	Landmarks	x	y	z	x	y	z	mm
T_{LB}	Anterior Commissure	0	-3	-1	-0.29	-2.94	-0.58	0.51
	Posterior Commissure	-1	10	-5	-0.84	10.44	-5.23	0.52
	Habenular Nuclei	-1	10	-1	-0.69	9.86	-1.02	0.34
T_{NLB}	Anterior Commissure	0	-3	-1	-0.35	-2.91	-0.58	0.55
	Posterior Commissure	-1	10	-5	-0.82	10.23	-5.27	0.40
	Habenular Nuclei	-1	10	-1	-0.64	9.58	-0.91	0.56

Table 2. Internal subject mean and maximum distance of transformed landmarks from the true coordinate location in brain template space (in mm).

	Anterior Commissure		Posterior Commissure		Habenular Nuclei	
Templates	Mean	Max	Mean	Max	Mean	Max
T_{LB}	0.72	1.63	0.71	1.53	0.75	1.63
T_{NLB}	0.70	1.23	0.66	1.43	0.70	1.49

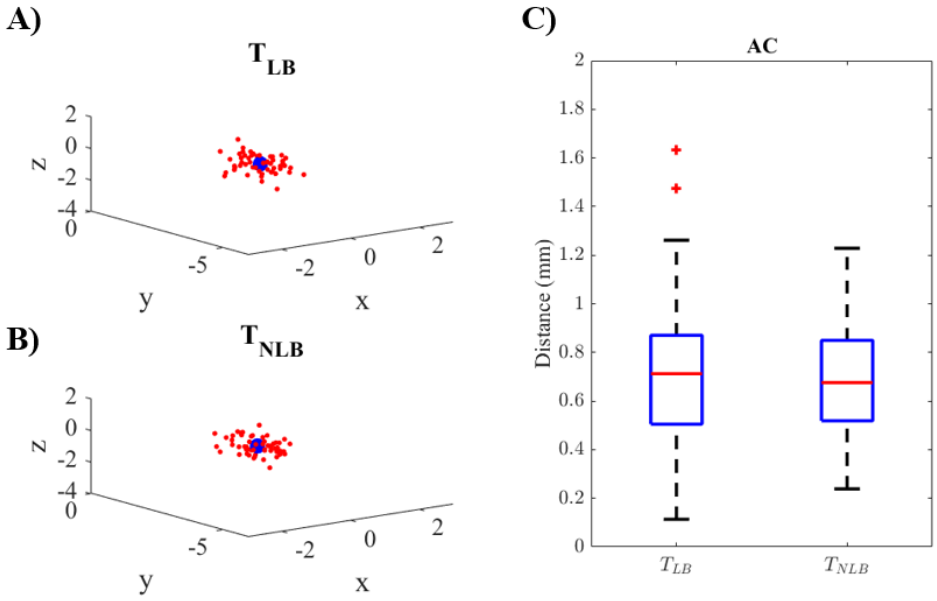

Figure 8. Internal template landmark variation of template subject AC (n=58) around the true mean (blue dot) in the **A)** linear brain template (T_{LB}) and **B)** non-linear brain template (T_{NLB}). **C)** Boxplot comparing the distribution around the true mean (in mm) where the red + signifies outliers.

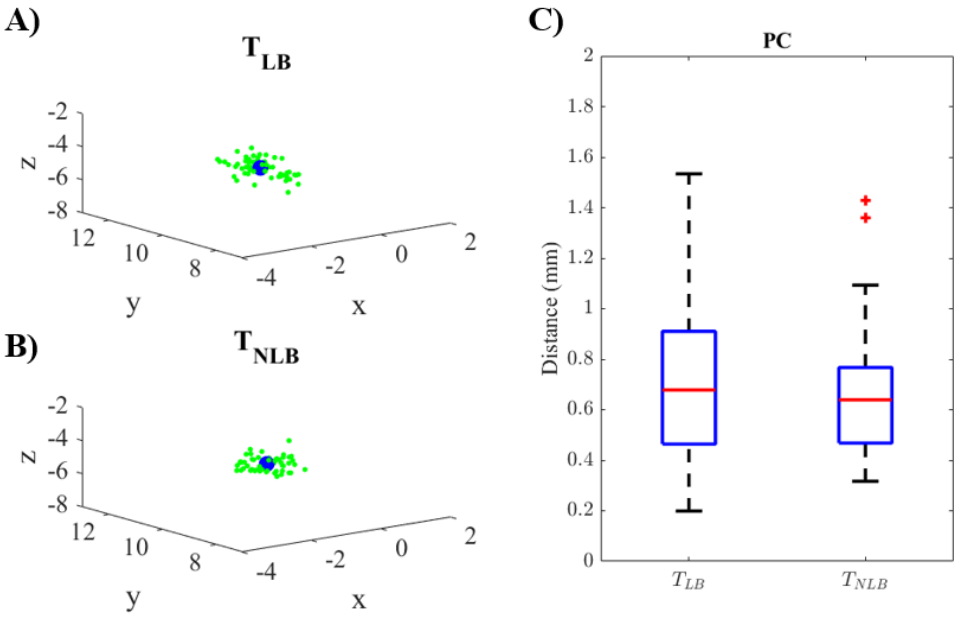

Figure 9. Internal template landmark variation of template subject PC (n=58) around the true mean (blue dot) in the **A)** linear brain template (T_{LB}) and **B)** non-linear brain template (T_{NLB}). **C)** Boxplot comparing the distribution around the true mean (in mm) where the red + signifies outliers.

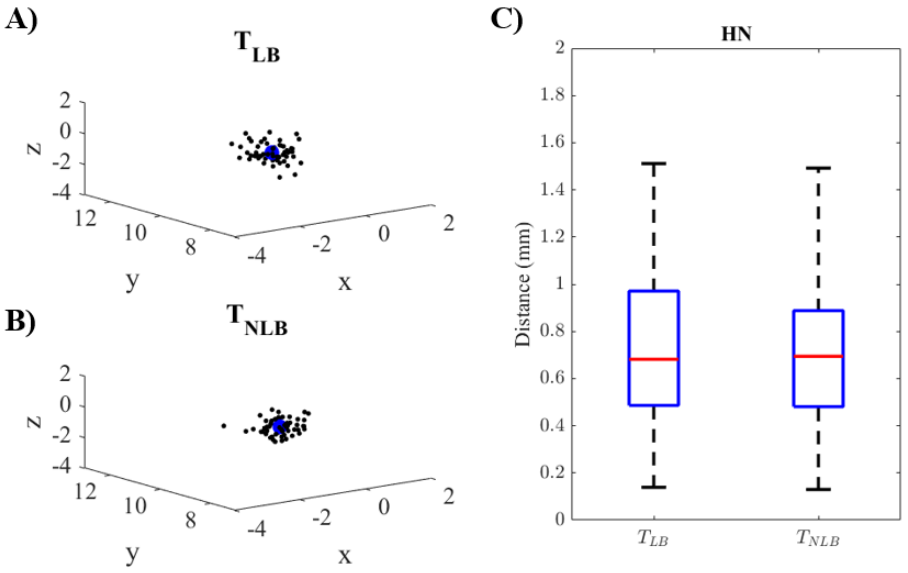

Figure 10. Internal template landmark variation of template subject HN (n=58) around the true mean (blue dot) in the **A)** linear brain template (T_{LB}) and **B)** non-linear brain template (T_{NLB}). **C)** Boxplot comparing the distribution around the true mean (in mm).

External Subject Landmark Variation

The AC, PC, and HN landmarks were selected in the original space for the 12 evaluation subjects that were not included in the template. After linear registration of the 12 subjects to each of the four templates, the transformation matrices were applied to the original selected points. Their distributions around the true coordinate, calculated during internal error measures, was plotted for each template and landmark in **Fig. 11** to **Fig. 13**. The mean and maximum distances from the true coordinate are reported in **Table 3**. Similar to the results from the internal subject landmark variation, the evaluation subject variation showed no significance in variation between the linear and non-linear template groups. However, the measured distances from the landmarks to the true coordinate in the brain template were significantly less than the landmark registration distances in the head template, indicating that the brain template performs more accurate registration ($p < 0.05$). Additionally, the external brain template landmark registration was not found to be significantly different from the internal brain template registration, validating that the developed brain template model performs as intended.

Table 3. External subject landmark mean and maximum distances from the true coordinate in all four template spaces (in mm).

	Anterior Commissure		Posterior Commissure		Habenular Nuclei	
Templates	Mean	Max	Mean	Max	Mean	Max
T_{LB}	0.79	1.38	0.74	1.86	1.09	1.45
T_{NLB}	0.76	1.16	0.95	2.00	1.19	1.79
T_{LH}	2.75	3.96	3.44	4.83	2.97	4.51
T_{NLH}	2.71	4.29	3.50	4.94	3.02	4.95

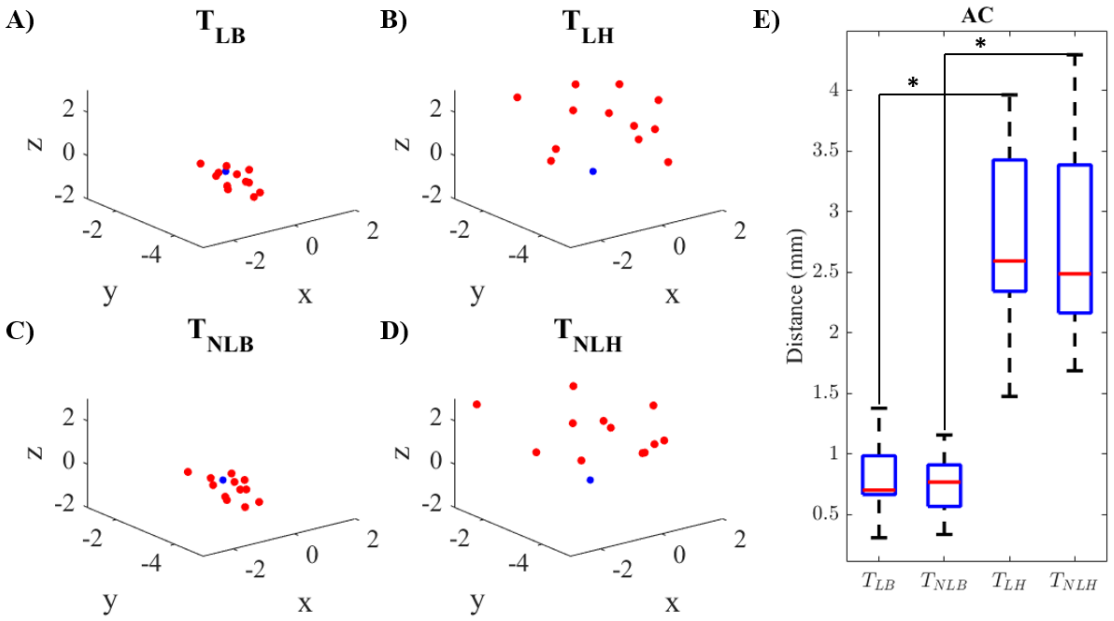

Figure 11. External subject landmark variation of the AC around the true mean (blue dot) in the **A)** linear brain template (T_{LB}), **B)** linear head template (T_{LH}), **C)** non-linear brain template (T_{NLB}), and **D)** non-linear head template (T_{NLH}). **E)** Boxplot comparing the distribution around the true mean (in mm) with significantly greater variation in the head templates compared to the brain templates (*p << 0.001).

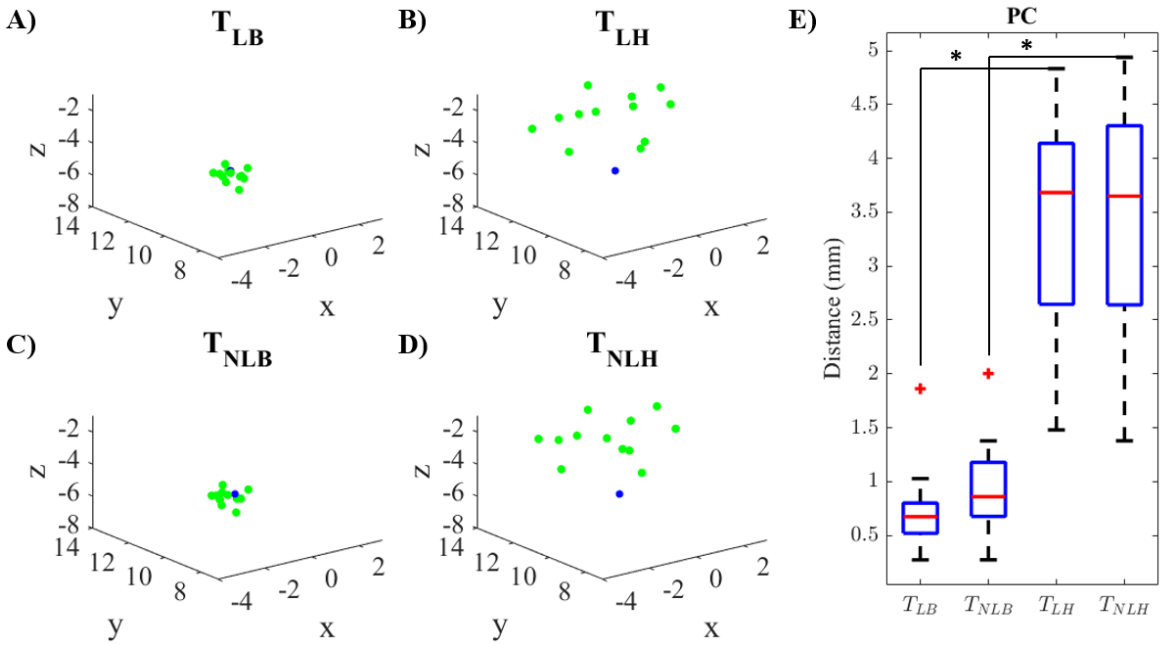

Figure 12. External subject landmark variation of the PC around the true mean (blue dot) in the **A)** linear brain template (T_{LB}), **B)** linear head template (T_{LH}), **C)** non-linear brain template (T_{NLB}), and **D)** non-linear head template (T_{NLH}). **E)** Boxplot comparing the distribution around the true mean (in mm) with significantly greater variation in the head templates compared to the brain templates (*p << 0.001) where the red + signifies an outlier.

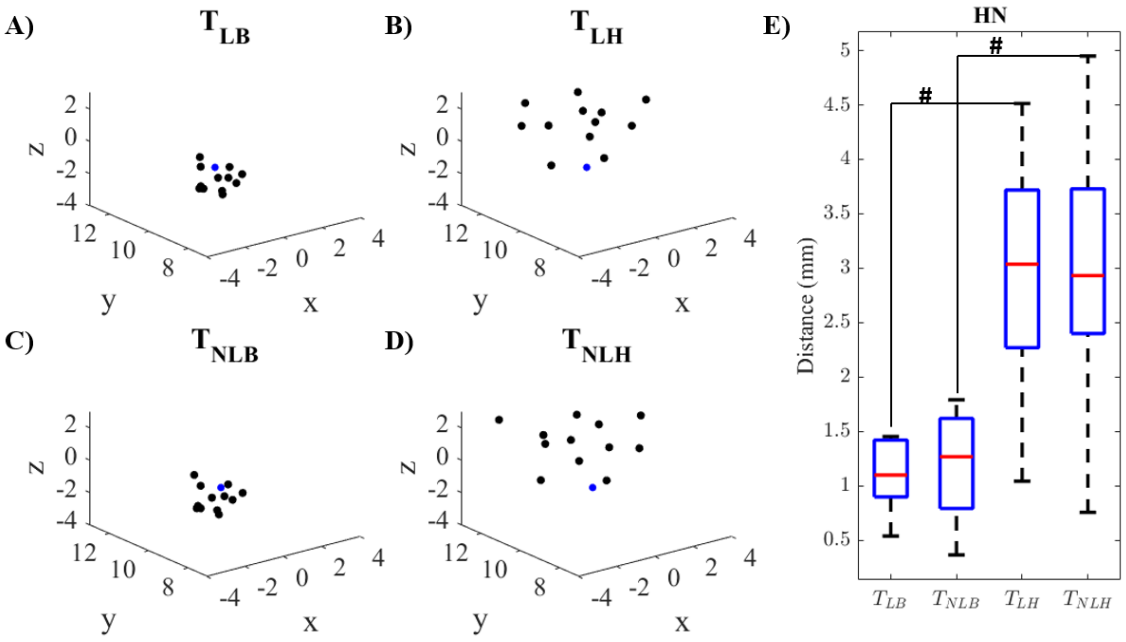

Figure 13. External subject landmark variation of the HN around the true mean (blue dot) in the **A)** linear brain template (T_{LB}), **B)** linear head template (T_{LH}), **C)** non-linear brain template (T_{NLB}), and **D)** non-linear head template (T_{NLH}). **E)** Boxplot comparing the distribution around the true mean (in mm) with significantly greater variation in the head templates compared to the brain templates (#p < 0.002).

Discussion

Two main templates were created: a brain template and a head template. Both templates provide a standardized space for Yucatan minipig brain recognition, and each provides its own benefits depending on the nature of its use. The created brain template is best suited to register skull-stripped, AC-PC aligned scans to allow for accurate structural registration to the template space, while the full head scan template is best suited to register AC-PC aligned full head scans with less structural accuracy. The measurement for structural variation within a newly created template is commonly determined using the AC and PC landmarks. The neonatal piglet template (n=15) showed a variation of about 0.41 and 0.65 mm for the average distances and 0.72 and 1.07 mm for the maximum distances between the internal subject and template AC and PC landmarks [31]. In a sheep brain template (n=18), created by Ella et al. (2015), the average distance from AC and PC points was about 0.44 and 0.56 mm with a maximum distance of 1.0 and 1.2 mm for the 12-parameter linear template [32]. Similarly, the 12-parameter rhesus macaque template (n=82) showed an average variation of 0.8 and 0.8 mm with maximum distances of 1.87 and 2.24 mm [35]. A noticeable increase in average and maximum variation occurs as the number of subjects included in the templates increases. Thus, for a template of 58, the average variation and maximum distribution for the AC and PC points in both the T_{LB} and T_{NLB} falls within the expected range with an overall maximum distance of 1.63 mm from the true landmark coordinate.

The T_{NLB} was found to have decreased template variance along the edges and increased spatial variance surrounding the internal structures. It is ideal for a majority of the template variance to be represented as internal structure variance. This property is likely enhanced in the non-linear template due to the smoothing or reduction of manual error around the external edges of the template by the warping functions. The non-linear template also showed increased voxel tissue probability in the CSF, GM, and WM segmented maps along with decreased internal landmark variation. Together all of these characteristics indicate that the non-linear template has a decreased and uniform internal statistical variance and structural variation.

The evaluation subject registration did not show that the T_{NLB} performed any better than the T_{LB}. Based on the study by Evans et al. (1992), templates with increased resolution lead to improved functionality [27]. Thus, the way to improve registration functionality in both linear and non-linear template registration would be to improve the template resolution. One way to increase the template resolution would be to increase the number of iterations in the recursive method [26]. With an increased number of iterations and an improved brain template, the resolution of the head templates is also expected to increase due to the

dependence of the head templates on the algorithms applied during brain template generation. This explains why the only thing in-focus in the head templates is the brain. Another way to improve the functionality of the head templates would be to begin a recursive method solely on the head scan now that a base head scan template exists. However, note that full head scans were successfully registered to the T_{NLB} in 11 of the 12 external subjects and with greater accuracy than to the T_{NLH}. This suggests that while the head templates have been created to register non-skull-stripped subjects, the T_{NLB} may still be the best option for accurate registration to template space.

The preprocessing steps of skull-stripping and inhomogeneity correction were key in reducing the amount of bias during registration. Even so, manual skull-stripping methods and marker selection for alignment to the AC-PC likely account for significant error in template functionality. This has the potential to be reduced in future non-human template creation with the creation of automated skull-stripping and AC-PC alignment algorithms for non-humans. Nonetheless, the number of subjects included in this template along with the narrow age range of the species provides outstanding power and ensures that the developed model effectively represents the population of interest.

Conclusions

The created brain templates perform in a similar manner when external subjects are registered, however, based on decreased variance, increased contrast in TPMs, and improved internal landmark registration, the T_{NLB} is recommended for template use to achieve the most accurate result. The publication of these templates is expected to provide accurate registration to a uniform coordinate space, ultimately allowing for group-level statistical comparisons and collaboration across research groups. Additionally, the methods outlined in this study create the potential for other researchers to develop their own species-specific templates. Future work will be performed using this template space to analyze the Yucatan minipig brain following blast exposure. With these templates, researchers will be able to use MRI as a tool to quantify, parameterize, and characterize brain mechanisms in controlled populations.

Appendix A

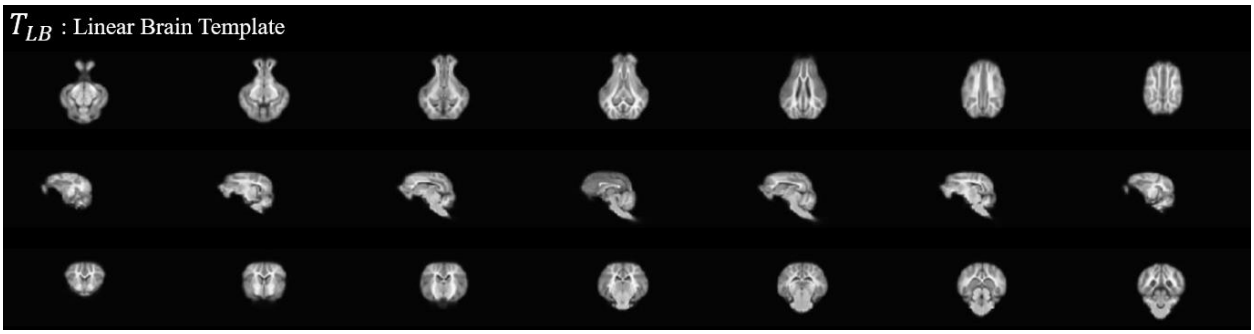

Figure A1. Linear brain template axial, sagittal, and coronal views across 4 mm slices.

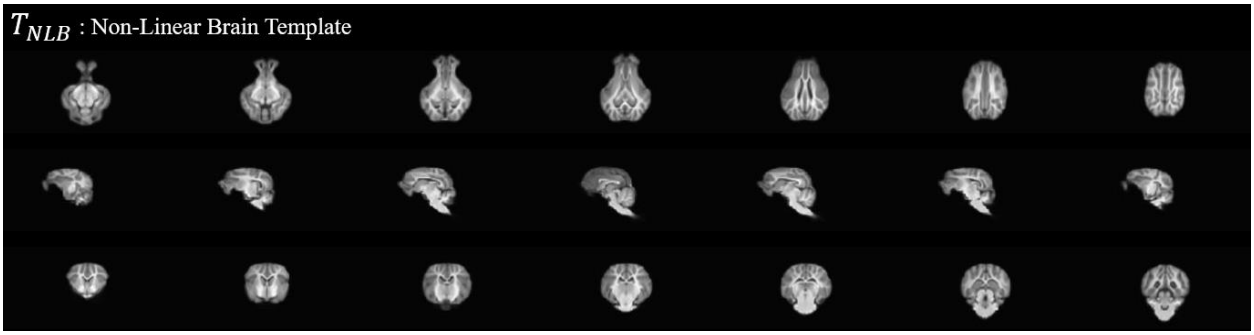

Figure A2. Non-linear brain template axial, sagittal, and coronal views across 4 mm slices.

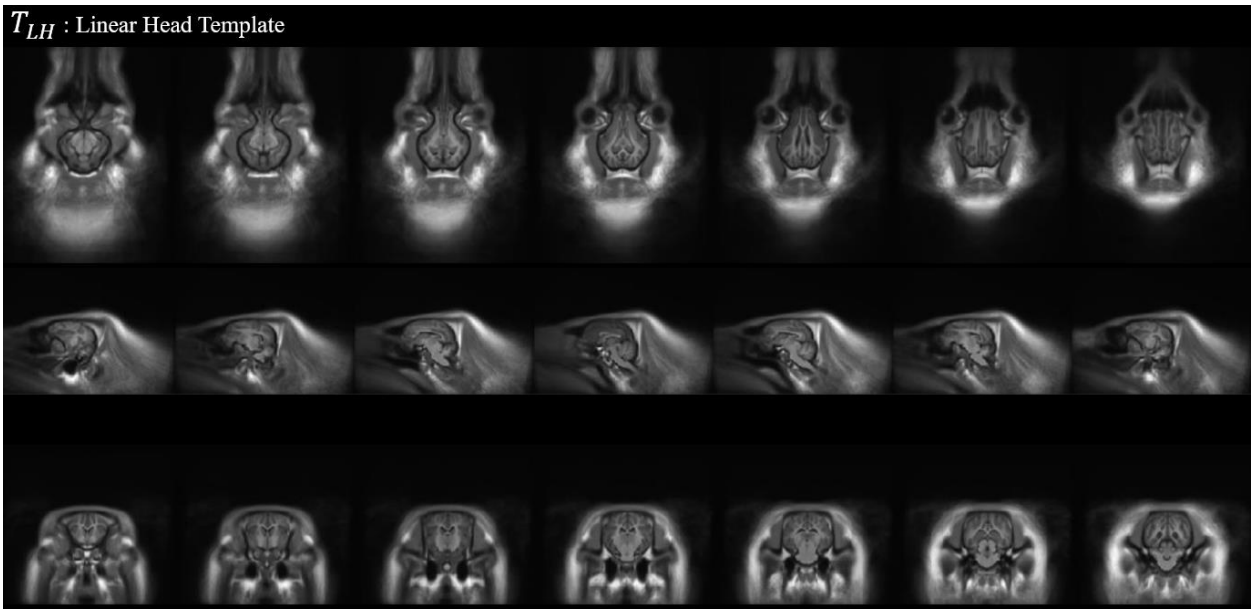

Figure A3. Linear head template axial, sagittal, and coronal views across 4 mm slices.

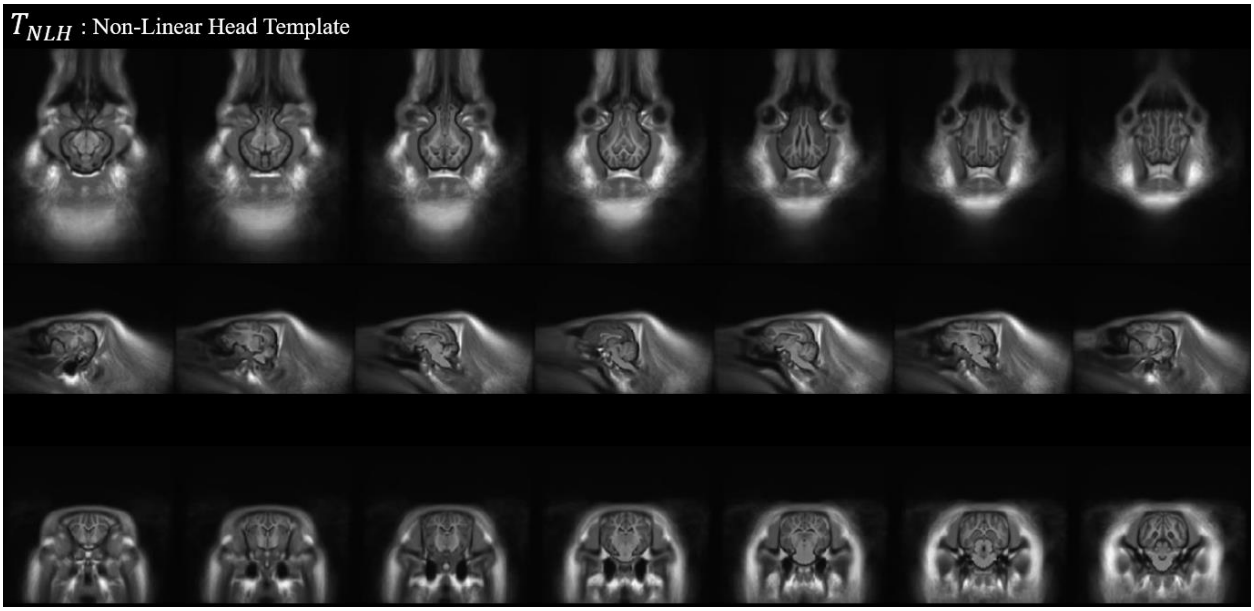

Figure A4. Non-linear brain template axial, sagittal, and coronal views across 4 mm slices.

References

[1] J. A. Goodrich *et al.*, "Neuronal and glial changes in the brain resulting from explosive blast in an experimental model," *Acta Neuropathologica Communications*, vol. 4, no. 1, p. 124, 2016/11/24 2016.

[2] M. Khoshnevis *et al.*, "Development of induced glioblastoma by implantation of a human xenograft in Yucatan minipig as a large animal model," *Journal of Neuroscience Methods*, vol. 282, pp. 61-68, 2017/04/15/ 2017.

[3] S. R. Platt *et al.*, "Development and characterization of a Yucatan miniature biomedical pig permanent middle cerebral artery occlusion stroke model," *Experimental & Translational Stroke Medicine*, vol. 6, no. 1, p. 5, 2014/03/23 2014.

[4] J. P. Mugler, 3rd and J. R. Brookeman, "Three-dimensional magnetization-prepared rapid gradient-echo imaging (3D MP RAGE)," (in eng), *Magn Reson Med*, vol. 15, no. 1, pp. 152-7, Jul 1990.

[5] R. W. Cox, "AFNI: software for analysis and visualization of functional magnetic resonance neuroimages," (in eng), *Comput Biomed Res*, vol. 29, no. 3, pp. 162-73, Jun 1996.

[6] S. M. Smith *et al.*, "Advances in functional and structural MR image analysis and implementation as FSL," (in eng), *Neuroimage*, vol. 23 Suppl 1, pp. S208-19, 2004.

[7] D. A. Dickie *et al.*, "Whole Brain Magnetic Resonance Image Atlases: A Systematic Review of Existing Atlases and Caveats for Use in Population Imaging," (in English), *Frontiers in Neuroinformatics*, Review vol. 11, no. 1, 2017-January-19 2017.

[8] E. Courchesne *et al.*, "Normal brain development and aging: quantitative analysis at in vivo MR imaging in healthy volunteers," (in eng), *Radiology*, vol. 216, no. 3, pp. 672-82, Sep 2000.

[9] C. D. Good, I. S. Johnsrude, J. Ashburner, R. N. Henson, K. J. Friston, and R. S. Frackowiak, "A voxel-based morphometric study of ageing in 465 normal adult human brains," (in eng), *Neuroimage,* vol. 14, no. 1 Pt 1, pp. 21-36, Jul 2001.

[10] R. C. Gur *et al.,* "Gender differences in age effect on brain atrophy measured by magnetic resonance imaging," *Proceedings of the National Academy of Sciences of the United States of America,* vol. 88, no. 7, pp. 2845-2849, 1991.

[11] E. R. Sowell, B. S. Peterson, P. M. Thompson, S. E. Welcome, A. L. Henkenius, and A. W. Toga, "Mapping cortical change across the human life span," (in eng), *Nat Neurosci,* vol. 6, no. 3, pp. 309-15, Mar 2003.

[12] J. Matsuzawa *et al.,* "Age-related volumetric changes of brain gray and white matter in healthy infants and children," (in eng), *Cereb Cortex,* vol. 11, no. 4, pp. 335-42, Apr 2001.

[13] D. A. Dickie *et al.,* "Progression of White Matter Disease and Cortical Thinning Are Not Related in Older Community-Dwelling Subjects," *Stroke,* vol. 47, no. 2, pp. 410-416, 2016.

[14] D. A. Dickie *et al.,* "Vascular risk factors and progression of white matter hyperintensities in the Lothian Birth Cohort 1936," (in eng), *Neurobiol Aging,* vol. 42, pp. 116-23, Jun 2016.

[15] H. Lemaitre, F. Crivello, B. Grassiot, A. Alperovitch, C. Tzourio, and B. Mazoyer, "Age- and sex-related effects on the neuroanatomy of healthy elderly," (in eng), *Neuroimage,* vol. 26, no. 3, pp. 900-11, Jul 1 2005.

[16] C. Farrell *et al.,* "Development and initial testing of normal reference MR images for the brain at ages 65-70 and 75-80 years," (in eng), *Eur Radiol,* vol. 19, no. 1, pp. 177-83, Jan 2009.

[17] J. M. Wardlaw *et al.,* "Neuroimaging standards for research into small vessel disease and its contribution to ageing and neurodegeneration," (in eng), *Lancet Neurol,* vol. 12, no. 8, pp. 822-38, Aug 2013.

[18] P. T. Fillmore, M. C. Phillips-Meek, and J. E. Richards, "Age-specific MRI brain and head templates for healthy adults from 20 through 89 years of age," *Frontiers in aging neuroscience*, vol. 7, pp. 44-44, 2015.

[19] S. P. Yun *et al.*, "Magnetic resonance imaging evaluation of Yukatan minipig brains for neurotherapy applications," *Laboratory Animal Research*, vol. 27, no. 4, pp. 309-316, 12/19

[20] N. M. Lind, A. Moustgaard, J. Jelsing, G. Vajta, P. Cumming, and A. K. Hansen, "The use of pigs in neuroscience: modeling brain disorders," (in eng), *Neurosci Biobehav Rev*, vol. 31, no. 5, pp. 728-51, 2007.

[21] R. Schubert *et al.*, "Neuroimaging of a minipig model of Huntington's disease: Feasibility of volumetric, diffusion-weighted and spectroscopic assessments," (in eng), *J Neurosci Methods*, vol. 265, pp. 46-55, May 30 2016.

[22] M. M. Swindle, A. Makin, A. J. Herron, F. J. Clubb, and K. S. Frazier, "Swine as Models in Biomedical Research and Toxicology Testing," *Veterinary Pathology*, vol. 49, no. 2, pp. 344-356, 2012/03/01 2011.

[23] K. L. Helke *et al.*, "Background Pathological Changes in Minipigs: A Comparison of the Incidence and Nature among Different Breeds and Populations of Minipigs," (in eng), *Toxicol Pathol*, vol. 44, no. 3, pp. 325-37, Apr 2016.

[24] F. Rosendal *et al.*, "MRI protocol for in vivo visualization of the Gottingen minipig brain improves targeting in experimental functional neurosurgery," (in eng), *Brain Res Bull*, vol. 79, no. 1, pp. 41-5, Apr 6 2009.

[25] C. R. Bjarkam, G. Cancian, A. N. Glud, K. S. Ettrup, R. L. Jørgensen, and J.-C. Sørensen, "MRI-guided stereotaxic targeting in pigs based on a stereotaxic localizer box fitted with an isocentric frame and use of SurgiPlan computer-planning software," *Journal of Neuroscience Methods*, vol. 183, no. 2, pp. 119-126, 2009/10/15/ 2009.

[26] A. C. Evans, A. L. Janke, D. L. Collins, and S. Baillet, "Brain templates and atlases," *NeuroImage,* vol. 62, no. 2, pp. 911-922, 2012/08/15/ 2012.

[27] A. C. Evans *et al.*, "Anatomical mapping of functional activation in stereotactic coordinate space," *NeuroImage,* vol. 1, no. 1, pp. 43-53, 1992/08/01/ 1992.

[28] D. L. Collins, P. Neelin, T. M. Peters, and A. C. Evans, "Automatic 3D intersubject registration of MR volumetric data in standardized Talairach space," (in eng), *J Comput Assist Tomogr,* vol. 18, no. 2, pp. 192-205, Mar-Apr 1994.

[29] J. Mazziotta *et al.*, "A probabilistic atlas and reference system for the human brain: International Consortium for Brain Mapping (ICBM)," *Philosophical transactions of the Royal Society of London. Series B, Biological sciences,* vol. 356, no. 1412, pp. 1293-1322, 2001.

[30] J. F. P. Ullmann, A. L. Janke, D. Reutens, and C. Watson, "Development of MRI-based atlases of non-human brains," *Journal of Comparative Neurology,* vol. 523, no. 3, pp. 391-405, 2015.

[31] M. S. Conrad, B. P. Sutton, R. N. Dilger, and R. W. Johnson, "An In Vivo Three-Dimensional Magnetic Resonance Imaging-Based Averaged Brain Collection of the Neonatal Piglet (Sus scrofa)," *PLOS ONE,* vol. 9, no. 9, p. e107650, 2014.

[32] A. Ella and M. Keller, "Construction of an MRI 3D high resolution sheep brain template," (in eng), *Magn Reson Imaging,* vol. 33, no. 10, pp. 1329-1337, Dec 2015.

[33] K. Hikishima *et al.*, "Population-averaged standard template brain atlas for the common marmoset (Callithrix jacchus)," *NeuroImage,* vol. 54, no. 4, pp. 2741-2749, 2011/02/14/ 2011.

[34] S. A. Love *et al.*, "The average baboon brain: MRI templates and tissue probability maps from 89 individuals," *NeuroImage,* vol. 132, pp. 526-533, 2016/05/15/ 2016.

[35] D. G. McLaren *et al.*, "A population-average MRI-based atlas collection of the rhesus macaque," (in eng), *Neuroimage,* vol. 45, no. 1, pp. 52-9, Mar 1 2009.

[36] B. Nitzsche *et al.*, "A stereotaxic breed-averaged, symmetric T2w canine brain atlas including detailed morphological and volumetrical data sets," (in eng), *Neuroimage,* Jan 31 2018.

[37] A. Ella, J. A. Delgadillo, P. Chemineau, and M. Keller, "Computation of a high-resolution MRI 3D stereotaxic atlas of the sheep brain," (in eng), *J Comp Neurol,* vol. 525, no. 3, pp. 676-692, Feb 15 2017.

[38] S. Saikali *et al.*, "A three-dimensional digital segmented and deformable brain atlas of the domestic pig," *Journal of Neuroscience Methods,* vol. 192, no. 1, pp. 102-109, 2010/09/30/ 2010.

[39] H. Watanabe, F. Andersen, C. Z. Simonsen, S. M. Evans, A. Gjedde, and P. Cumming, "MR-Based Statistical Atlas of the Göttingen Minipig Brain," *NeuroImage,* vol. 14, no. 5, pp. 1089-1096, 2001/11/01/ 2001.